A Convenient Route to Modified Multiwall Carbon Nanotubes with Liquid Crystal Molecules via Covalent Functionalization

Xianhong Chen,[1] Xiaoli Wu,[1] Jiagui Zou,[1] Jianping Wan[2]

[1]*College of Materials Science and Engineering, Hunan University, Changsha 410082, People's Republic of China*
[2]*Hunan Communications Research Institute, Changsha 410015, People's Republic of China*

Received 8 June 2010; accepted 26 July 2011
DOI 10.1002/app.35358
Published online 21 November 2011 in Wiley Online Library (wileyonlinelibrary.com).

ABSTRACT: A novel nanocomposite of the rod-like liquid crystal (LC) molecules' waist positions anchored on the surface (sidewalls and ends) of multiwall carbon nanotubes (MWNTs) was prepared by using a dissolving metal reduction method for the first time. The MWNTs carbanion complexes of lithium were first synthesized in tetrahydrofuran with an electron transfer from lithium naphthalene radical anion on the surface of MWNTs. Then the novel material (LC-MWNTs) was obtained by treating the carbanion complexes with bromic liquid crystalline aromatic amide compound. The formation of the LC-MWNTs was confirmed by both Raman and FTIR spectroscopies. HRTEM demonstrates that the rod-like LC molecules are anchored on the surface of MWNTs via covalent attachment, with a wrapped thickness approximately 3-4 nm. The loss-weight fraction of the LC layers for the LC-MWNTs can be roughly estimated as 23% by TGA. The experiments of solubility exhibit that the LC-MWNTs forms a stable suspension solution in polar solvents such as dimethylformamide. © 2011 Wiley Periodicals, Inc. J Appl Polym Sci 124: 3399–3406, 2012

Key words: multiwall carbon nanotubes; liquid crystal; modification; nanocomposites; TEM

INTRODUCTION

Because of carbon nanotubes (CNTs) unusual chemical structure and intriguing physical properties, its composites have became a matter of intensive research in the last decades.[1–5] Because liquid crystals (LC) exhibit long-range orientational order along a special direction, it seems feasible to exploit the self-organizing properties of LC to induce the alignment of dispersed CNTs. And combination of CNTs with LC was particularly interesting in recent years.[6–10] It has been reported that a minute addition of carbon nanosolids such as C_{60} and multiwall carbon nanotubes (MWNTs) dispersed in LC affects the electro-optical properties and response time of the cell.[11] Koysal et al. reported the maximum diffraction efficiency enhanced from 7% for pure nitrile-ester mixture LC to 15% for CNTs/LC composite containing only 0.05 wt % nanotubes.[12] Jou et al. reported that the electromagnetic shielding effectiveness in CNTs/LC polymers composite was 62.1 dB which is realistic for an industrial application.[13] The promising applications of the magnetically steered electrical switch device based on CNTs/LC(E7) composite was recently demonstrated.[14]

New composites providing novel mechanical, electrochemical, electronic, and optical capabilities may arise from the molecular-level interaction between CNTs and different matrices with high performance and multifunction.[4,5] So good dispersion and interfacial binding are the necessary conditions for CNTs/LC composite with higher performance and multifunction.[10] Some methods have been proposed to overcome the various barriers for accomplishing dispersion of CNTs including the use of ultrasonication,[6,8,15] high shear mixing, the aid of surfactants, and combinations of these.[7,16] Up to now, however, very limited success for CNTs/LC composites has been achieved, mainly because of poor compatibility between CNTs and LC cells.[17] Functionalization of CNTs via covalent attachment of chemical groups such as anchoring various LC molecules, is essential to improve the interfacial strength and dispersion of CNTs in LC matrix. Covalent functionalization of CNTs based on either the

Correspondence to: X. Chen (xianhongchen@hnu.cn).
Contract grant sponsor: Innovation Fund for Technology Based Firms; contract grant number: 09C26214301994.
Contract grant sponsor: Science and Technology Planning Project of Changsha City; contract grant number: K1005176-11.
Contract grant sponsor: Innovation program of Science and Technology in Transportation Commission of Hunan Province; contract grant number: 200814.
Contract grant sponsor: Aid Program for Science and Technology Innovative Research Team in Higher Educational Institutions of Hunan Province.

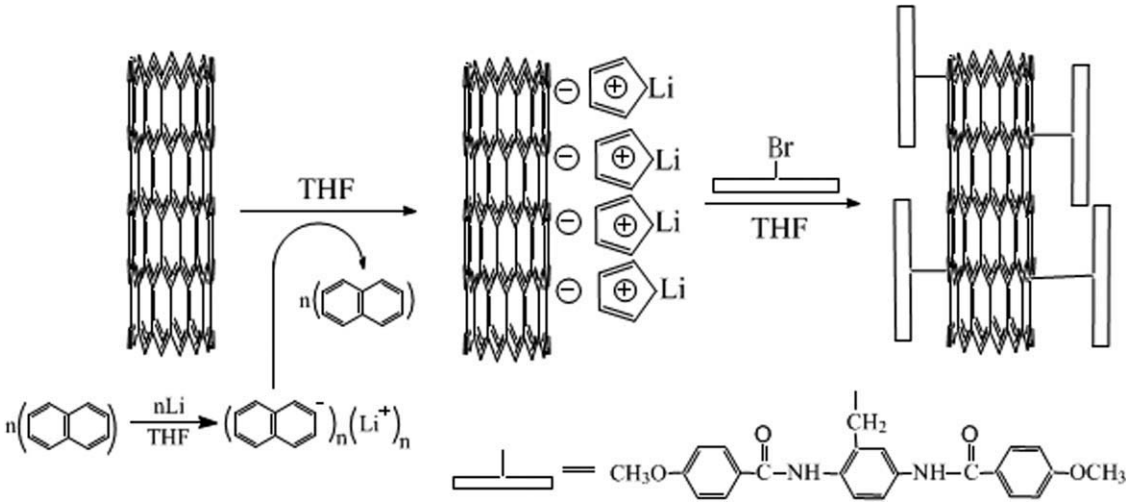

Scheme 1 Illustration for the synthesis routes of LC-MWNTs nanocomposite.

nanotube-bound carboxylic acid moieties or the sidewall addition has commonly been used. The previous one has been explored through oxidation routes that lead to shorten nanotubes and destroy the layer structure.[18] Reagents added to the sidewalls include fluorine,[19] azomethine ylides,[20] organo-lithium,[21] nitrenes,[22] carbenes,[23] radicals,[24] aryl diazonium salts,[25] and Billups reaction.[26] Recently, a dissolving metal reduction method has been reported.[27–29]

In this contribution, a novel LC-MWNTs was synthesized facilely (Scheme 1) by means of the dissolving metal reduction method to anchor the rod-like LC molecules (2-methyl-*N,N*′-bis(4′-methoxy benzoyloxy)-terephthalamide) via their waist positions on the sidewalls and ends of MWNTs for the first time. The LC-MWNTs was prepared only in one-step reaction after obtaining the rod-like LC compound. Covalent functionlization of MWNTs with LC molecules is regarded as promising in creating new functional nanohybrids since it not only provides a chance to combine the advantages of both, but also affords an opportunity to generate novel characteristics. It will have a great of potential applications like photoconductors, light-emitting diodes, photovoltaic solar cells, sensors, optical data storage, and thin-film transistors. Meanwhile, this research is one part of a larger project on the development of surface treatment techniques for CNTs/LC composite. This method provides an accommodating, direct, cheap, scalable, and efficient route to functionalize MWNTs by groups that are suitable for further elaboration.

EXPERIMENTAL

Materials

The raw MWNTs used in this work was prepared by the chemical catalytic vapor deposition process (CCVD).[30] As-prepared product was purified with a mixture of sulfuric acid and nitric acid (3:1 by volume) in a sonication bath (40 kHz) at 70°C for 8 h. 2,5-Diaminotoluene sulfate, *p*-methoxybenzoic acid, triphenyl phosphine, and *N*-bromosuccinimide (NBS) were purchased from Aldrich. Potassium hydroxide, hexachloroethane, pyridine, *N,N*′-dimethylformamide (DMF), tetrahydrofuran (THF), benzoyl peroxide, lithium, benzene, and naphthalene were purchased from Shanghai Chemical Reagent Corp. All reagents were used as received.

Characterization

Fourier transform infrared spectrum (FTIR) measurements were performed on a WQF-410 FTIR spectrometer in the range of 400–4000 cm^{-1} at the resolution of 2.0 cm^{-1}. All of the samples for FTIR measurements were deposited on the surface of a KBr plate. Hydrogen nuclear magnetic resonance (^{1}H-NMR) spectrum was obtained with a Bruker ARX400 spectrometer by using dimethyl sulfoxide (DMSO) as solvent and tetramethylsilicone (TMS) as internal standard. An Olympus BX 51 polarizing light microscopic (POM) equipped with a Mettler FP82HT hot stage was used to observe the optical textures of LC. Raman spectroscopy measurements were recorded on the Laser Confocal Raman spectroscopy (JOBINYVON Labram-010, 632.8 nm excitation). High-resolution transmission electron microscopy (HRTEM) images were obtained on a JEOL-3010 ultrahigh resolution transmission electron microscope. Thermogravimetric analysis (TGA) of purified MWNTs and LC-MWNTs was performed using NETZSCH STA-409 analyzer. These experiments were carried out with 15 mg of specimen placed in a TGA pan and heated at 10°C/min up to 680°C in a flow of nitrogen.

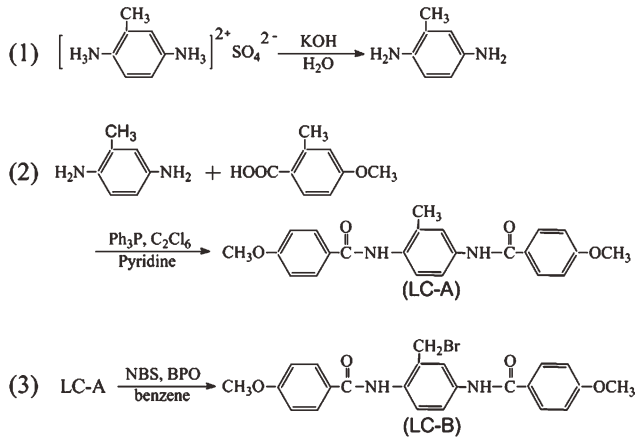

Scheme 2 Illustration for the synthesis routes of LC-A and LC-B.

Synthesis of LC and its derivative

The synthesis routes of the liquid crystalline compound and its derivative are shown in Scheme 2. The synthesis involved three steps, and the experimental details are described below.

2,5-Diaminotoluene sulfate (30 g, 0.1 mol) was dissolved in 110 mL potassium hydroxide solution (1 mol/L). The solution was extracted with four 250 mL aliquots of chloroform. Then the chloroform extracts were dried over magnesium sulfate, filtered, and then evaporated to dryness, yielding a white solid of the crude 2,5-diaminotoluene (11.5 g, 69%), which was used without further purification.

p-Methoxybenzoic acid (6.1 g, 0.04 mol) and triphenyl phosphine (12.6 g, 0.048 mol) were dissolved in 25 mL dried pyridine to obtain solution A. 2,5-Diaminotoluene (2.3 g, 0.019 mol) and hexachloroethane (14.2 g, 0.06 mol) were dissolved in 35 mL of dried pyridine to obtain solution B. B was rapidly added into A, and the mixture was strongly stirred at room temperature for 5 h. Subsequently, the mixture was poured into ethanol to precipitate the product, which was collected and washed successively with acetone, distilled water, and ether in turn. Finally, the product was further purified by recrystallization in a 7:3 mixture of DMF and distilled water, yielding 6.4 g (86.2%) 2-methyl- *N,N*′-bis(4′-methoxy benzoyloxy)-terephthalamide (LC-A).

A flask fitted with a reflux condenser was charged with 7.9 g (20 mmol) of LC-A, 3.7 g (21 mmol) of NBS, 0.2 g (8 mmol) of benzoyl peroxide, and 150 mL of dry benzene. The mixture was refluxed for 8 h. After filtration of insoluble materials from the mixture, the solution containing products was washed successively with water and then dried with anhydrous sodium sulfate. Subsequently, the benzene solution was concentrated on a rotary evaporator to leave a light yellow needle crystal-crude product. Finally, recrystallization of the crude product in a 1:1 mixture of ethanol and benzene, yield 7.2 g (75.8%) of pure LC-B.

Synthesis of LC-MWNTs

The preparation of LC-MWNTs was carried out as follows: 20 mg (1.6 mmol of carbon) of MWNTs was added to a flame-dried 100 mL three-neck round-bottom flask. THF (60 mL) was then condensed into the flask followed by the addition of small pieces of lithium metal (231 mg, 33 mmol) and naphthalene (2.31 g, 18 mmol), and the deep green reaction mixture was vigorous stirred in a sonication bath (40 kHz) for 6 h. Then, LC-B (2 g, 4.26 mmol) was added to the reactants. After 24 h, the reaction mixture was filtered using 0.22-μm pore size polyvinylidene fluoride filter paper. Subsequently, the residue was washed with a large amount of THF, DMF, benzene and water. Finally, product of LC-MWNTs was obtained after vacuum drying at 80°C overnight.

RESULTS AND DISCUSSION

Characterizations of LC molecule and derivative

The structure of the LC-A was confirmed by FTIR and ^{1}HNMR spectroscopy. The FTIR spectrum of LC-A (Fig. 1) shows two strong bands at 3290 and 1641 cm^{-1}, which correspond to the *N*—H and C=O stretching vibrations, respectively. The peak at 1302 cm^{-1} refers to C—N stretching and peak at 681 cm^{-1} is assigned to *N*—H bending. The arc-H stretching is observed in the range of 2840–3000 cm^{-1}. The peaks at 1446 and 1254 cm^{-1} are attributed to C—H bending of the arc-CH_3 group and C—O stretching of the arc-OCH_3 group, respectively. Further support for the structure of LC-A can be obtained from ^{1}HNMR spectrum recorded in DMSO-d6 (Fig. 2). The signals at 9.7–10.2, 7.0–8.0, 3.8, and 2.2 ppm correspond to NH-CO [2.01 H, Fig. 2(γ)], arc-H [10.37 H, Fig. 2(β)], arc-OCH_3 [6.20 H, Fig. 2(α)] and arc-CH_3 [2.63 H, Fig. 2(δ)], respectively. Both FTIR and ^{1}H-NMR demonstrate that LC-A has been prepared. The formation of LC-B was confirmed by FTIR measurements shown in Figure 1 (LC-B). It can be seen that LC-B and LC-A spectra show similar characteristic bands, but there is a slight difference. For LC-B, disappearance of characteristic peak of arc-CH_3 at about 1446 cm^{-1} and appearance of a new absorption peak at 1024 cm^{-1}, which is assigned to the presence of C-Br, indicate that the reaction of Scheme 2(3) has accomplished. Meanwhile, the liquid crystalline phases of LC-A and LC-B were investigated using POM. The samples which were sandwiched between a glass slide and a cover slip were heated to 281°C, and the textures were imaged during cooling under crossed polarizer. Figure 3(a,b)

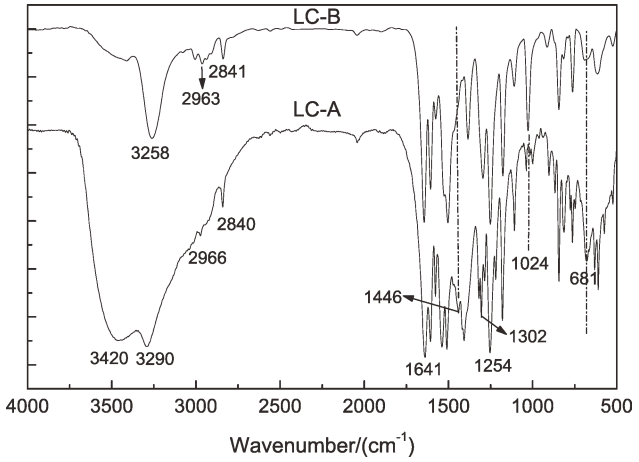

Figure 1 FTIR spectra of LC-A and LC-B.

are the POM images of LC-A at 280 and 274°C, respectively. They remarkably exhibit the fan-shaped textures which belong to the common characteristic of smectic A (SmA) phase.[31] These experiments show that LC-A melts at 268°C and forms a liquid-crystalline state. It is notable that liquid crystal behavior of LC-B is also quite similar to that of LC-A in our observation.

Characterizations of LC-MWNTs

Scheme 1 shows the synthesis routes of LC-MWNTs. MWNTs is reduced after an electron transfer from lithium naphthalene radical anion to the surface of MWNTs in THF. This results in a high level of coverage surrounding the carbon nanotubes by radical anions. Subsequently, the reduced MWNTs was functionalized by reaction of these radical anions with the bromo-LCs (LC-B), obtaining LC-MWNTs.

Raman spectroscopy provides essential and quick information for the evaluation of the covalent bond

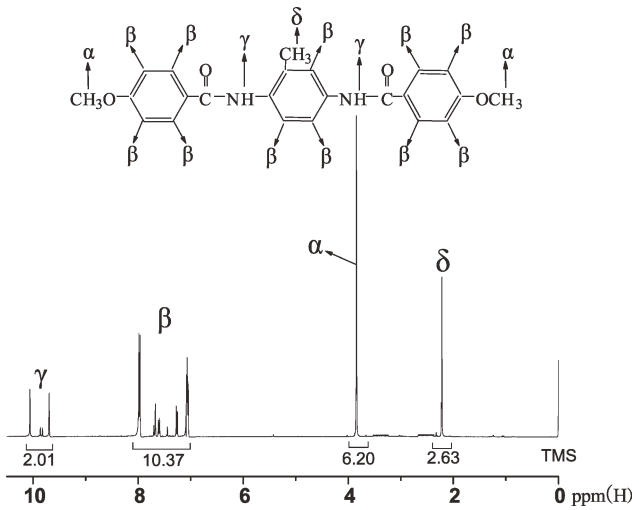

Figure 2 ^{1}H-NMR spectrum of LC-A.

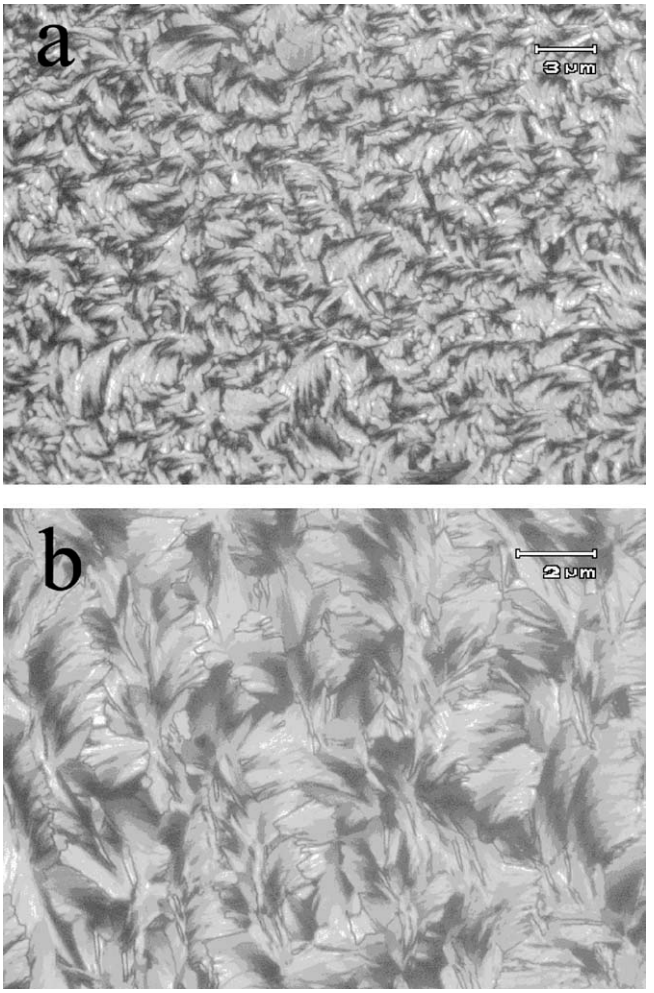

Figure 3 Polarized optical microscopic fan-shaped textures observed for LC-A obtained on cooling from isotropic liquid at 280°C (a) and 274°C (b).

connection of MWNTs. Figure 4 shows the Raman spectra of purified MWNTs and LC-MWNTs samples. It is clear that the D-, G-, and D′-bands can be

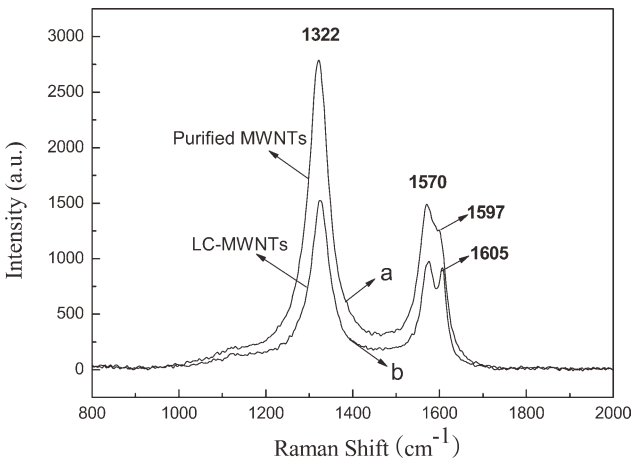

Figure 4 Raman spectra of purified MWNTs (a) and LC-MWNTs (b).

TABLE I
The Position and Relative Intensity Ratios of the D- to G-Bands (R_D/R_G) of Different Samples

Samples	ω_D[a]/cm^{-1}	ω_G[b]/cm^{-1}	ω_D[c]/cm^{-1}	R_D/R_G[d]
Purified MWNTs	1322	1570	1597	1.998
LC-MWNTs	1322	1575	1605	2.670

[a] The peak position of D-bands of MWNTs.
[b] The peak position of G-bands of MWNTs.
[c] The peak position of D′-bands of MWNTs.
[d] R_D and R_G are the intergrate area of D-bands and G-bands, respectively.

observed at about 1322, 1570, and 1597 cm^{-1} for two samples, respectively. G-band (at near 1570 cm^{-1}) corresponding to the tangential C—C stretching vibration is associated with the ordered sp^2 hybridized carbon network. D-band (at about 1322 cm^{-1}) is related to local defects that originate from structural imperfections and is involved with the scattering of an electron by phonon emission by the disordered sp^3 hybridized carbon network.[32,33] By contrast with purified MWNTs, the D′-band is very strong for LC-MWNTs. Meanwhile, the D′-band of LC-MWNTs slightly shifts downfield for near 8 cm^{-1}. Moreover, the relative intensity ratio of the D- and G-bands (R_D/R_G), which is widely used as a measure of surface covalent derivatization or defect introduction,[34] obviously increases from 1.998 for purified MWNTs to 2.670 for LC-MWNTs (Table I). It may arise from missing carbon atoms (vacancies), covalent bond formation, or disorder of any kind in the aromatic π-domain. As a result, the improved R_D/R_G should result from covalent bond connection (formation of the MWNTs-methene bond), in other words, a large number of sp^2 hybridized carbons have been converted into sp^3 hybridized atoms.

To get further information of LC-MWNTs, FTIR spectroscopy was conducted. Figure 5 shows the FTIR spectra of LC-B, purified MWNTs, and LC-MWNTs. As can be seen from the FTIR spectrum of LC-B, LC-B has characteristic bands of *N*—H at 3258, 1580, and 680 cm^{-1}, arc-H at 2840–3000, 837, and 751 cm^{-1}, C=O at 1645 cm^{-1}, C=C at 1605 and 1506 cm^{-1}, C—N at 1376 and 1302 cm^{-1}, arc-OCH_3 at 1254 cm^{-1}, C—O at 1150 and 1105 cm^{-1}, C-Br at 1024 cm^{-1}. For the purified MWNTs sample, the peak at 1699 cm^{-1} refers to the FTIR stretching vibration frequency of carboxylic acid groups (C=O) and the peak at 1516 cm^{-1} refers to carboxylate groups (—COO—) after oxidation treatment.[35] Compared with purified MWNTs, the FTIR spectrum of LC-MWNTs shows the mainly absorptions that are characteristic for LC molecules. The characteristic peaks of LC-MWNTs composite are at 3424, 1585, and 671 cm^{-1}, which are assigned to *N*—H stretching frequency. The peak of *N*—H stretching vibration is distinctly blue-shifted from 3258 to 3424 cm^{-1} in Figure 5(c), this is as a result of the disappearance of intermolecular hydrogen bond of LC-B which can be proved by the FTIR characteristic broad peak at approximately 3450 cm^{-1} [Fig. 5(a)]. The new peaks at 2800–3000, 1724, 1150, and 1083 cm^{-1} contribute to C—H, C=O, and C—O stretching vibrations, respectively. The peak at 1376 cm^{-1} is assigned to the stretching vibration of C—N. Associating FTIR with Raman spectra of LC-MWNTs, the disappearance of the characteristic peak (C-Br for LC-B at ~ 1024 cm^{-1}) in the LC-MWNTs composite spectrum further indicates that the reactions of Scheme 1 have been finished successfully, and LC-B has been successfully attached to the surface of MWNTs via covalent bonding formation.

The nanostructure of LC-MWNTs was then investigated by HRTEM. The specimens were prepared by applying a few drops of the sample solution (with the concentration of MWNTs of 0.3 mg/mL) onto a holey carbon-coated copper grid and then evaporating off the solvent. The HRTEM images are shown in Figure 6. At low magnifications, it seems that LC-MWNTs is dispersed well with few bundles [Fig. 6(b,c)], and the average length of the LC-MWNTs is about several micrometers. In the higher magnification micrographs [Fig. 6(d)], the core-shell nanostructure is observed clearly. As a comparison, no amorphous layers were observed in the image of purified MWNTs [Fig. 6(a)]. The carbon tube has been constructed from graphite lamella layer-by-layer, and the LC shell is vividly impinged on the outer wall along the tube stretched direction. The average thicknesses of the enwrapped LC layers are ~ 3 nm (measured from 8 to 10 tubes).

Additional evidence for covalent attachment of LC molecules onto the MWNTs has been provided by

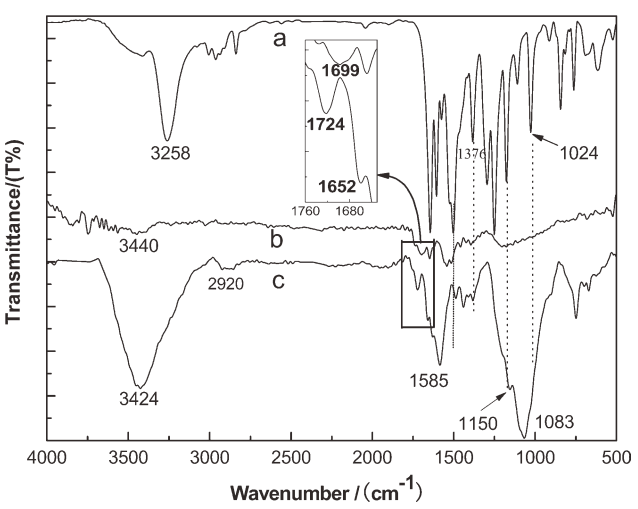

Figure 5 FTIR spectra of LC-B (a), purified MWNTs (b) and LC-MWNTs (c).

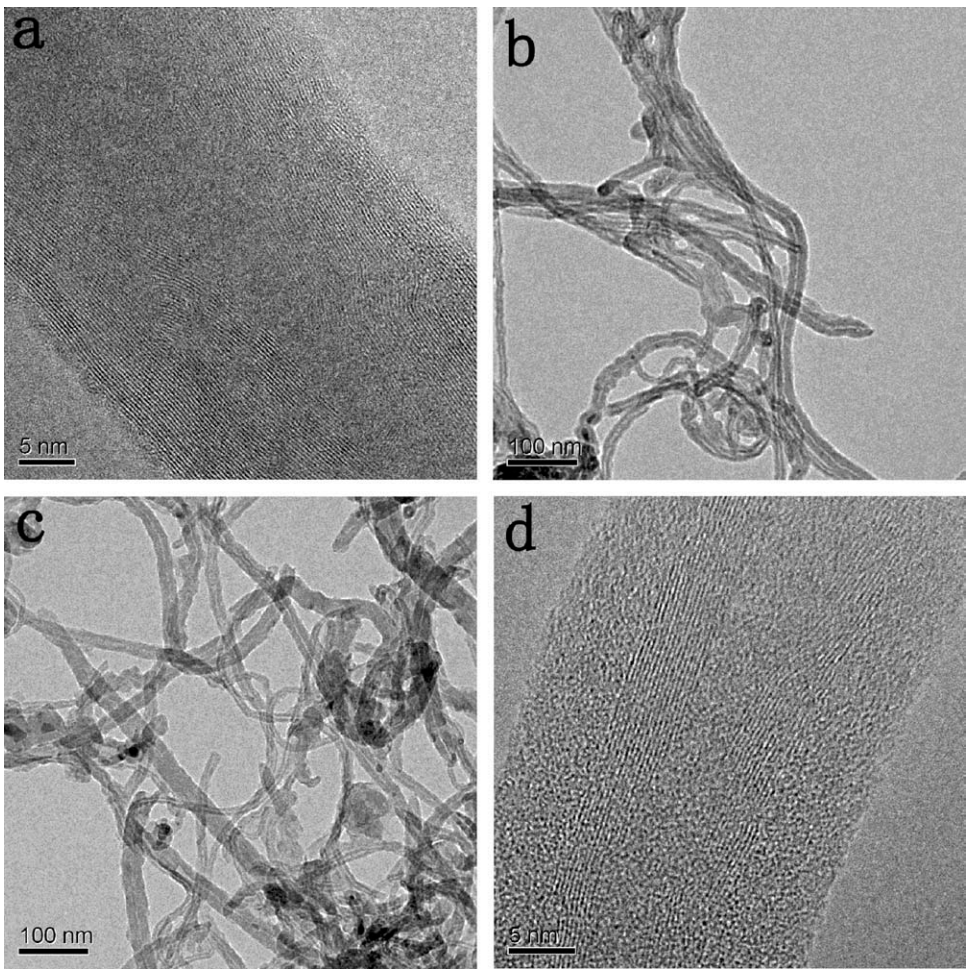

Figure 6 HRTEM images of purified MWNTs (a) and LC-MWNTs (b, c, d).

TGA of Figure 7 in the range of 50–680°C. For the purified MWNTs [Fig. 7(a)], it almost remains stable up to about 450°C and has only a 3–5% weight loss which is probably related to the removal of the attached carboxy group and hydroxyl group. The obvious loss starts at above 450°C, and the temperature of decomposition of the nanotube framework is about 550°C. The result is identical with that of our previous research.[25] For the LC-MWNTs sample [Fig. 7(b)], because of the decomposition of LC-A the small beginning weight loss occurred from 180°C, which is much lower than the decomposition temperature of neat LC-A [Fig. 7(c)]. The better thermal stability of LC-A is contributed to the strong hydrogen bond, which can be proved by the strong FTIR characteristic peak at 3500 cm^{-1}[Fig. 1(a)]. The thermal analysis of LC-MWNTs shows three weight loss steps. Below 359°C a 21% weight loss observed can be attributed to the presence of methoxy group or methyl of LC-A side group, and the second weight loss occurred between 359 and 455°C may be attributed to oxidative removal of the amide linkage of LC-A side group. These degradation appears to be delayed in pristine LC-A. The third rapid weight loss took place above 455°C due to the decomposition of MWNTs. With such a wide difference in stability it is possible to measure the amount of LC molecules in a given LC-MWNTs sample.[36] On the assumption that the weight loss is due to elimination of the LC moiety and the interactions between LC

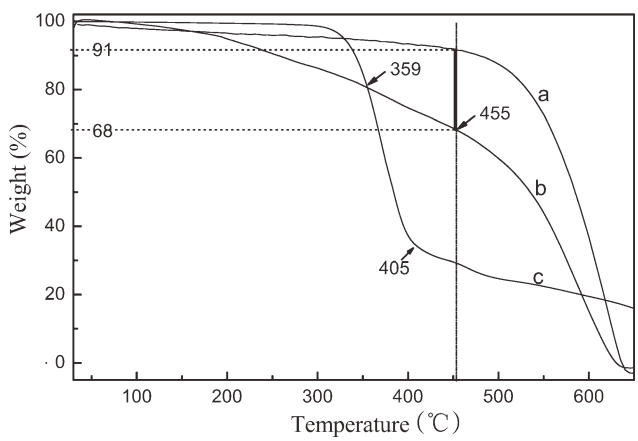

Figure 7 TGA trace of purified MWNTs (a), LC-MWNTs (b) and LC-A (c).

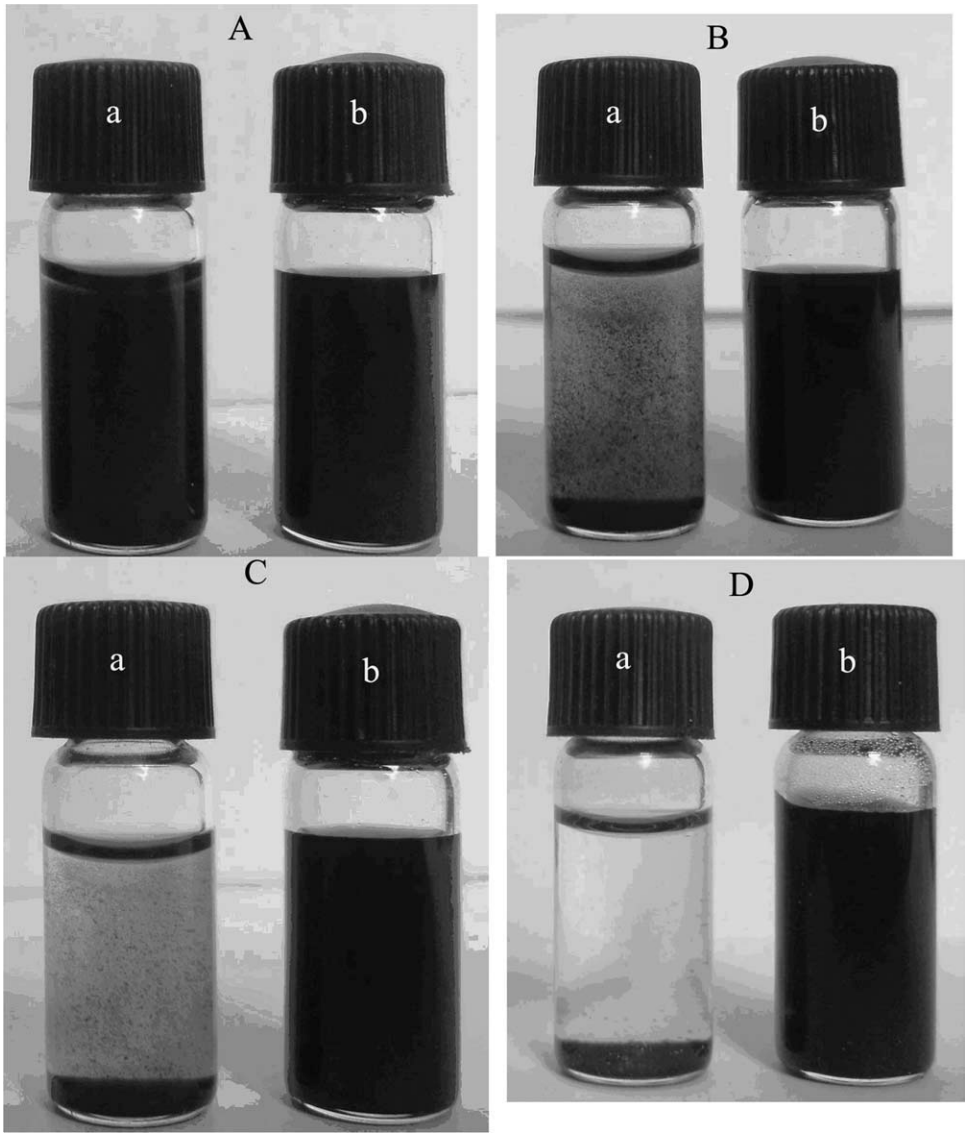

Figure 8 Photographs of LC-MWNTs (a) and purified MWNTs (b) in H_2O. Immediately after sonication (A), after 5 min (B), after 1 h (C), after 24 h (D).

molecules and MWNTs are ignored, by a referenced temperature standard of the decomposition of MWNTs, LC-MWNTs, and LC-A, the loss-weight fraction of the LC layers for the LC-MWNTs can be roughly estimated as 23% (Fig. 7).

The formation of stable suspensions of CNTs is a critical target in the development of practical applications of this valuable material. A quantitative comparison of the solubility of purified MWNTs and the LC-MWNTs in water (Fig. 8) and DMF (Fig. 9) was performed as follows: 1 mg of sample was dispersed in 5 mL of the selected solvent by ultrasonication for 0.5 h. Figure 8 demonstrates the stability of the dispersion of LC-MWNTs and purified MWNTs for 0 min, 5 min, 1 h, and 24 h after ultrasonication. It can be seen that there are great differences between purified MWNTs and LC-MWNTs in water. The purified MWNTs exhibits good stability of the dispersion in water [Fig. 8(b)]. In reverse, the stability of the dispersion of LC-MWNTs becomes poorer and poorer after prolonged standing [Fig. 8(a)]. The sedimentation at the bottom of the vial can be observed after ultrasonication for 24 h [Fig. 8(D)]. The difference may be caused by the good or poor solubility of both materials in water. For the purified MWNTs, some carboxylic acid groups on the surfaces of MWNTs significantly improve the solubility of purified MWNTs in water, and form a homogenous suspension. For the LC-MWNTs, the compatibility between LC molecule of LC-MWNTs and water is quite poor, therefore the solution is unstable and it easily results in phase separation. It is worthy to be noted that both purified MWNTs and LC-MWNTs display good suspendability in DMF even after a month (Fig. 9). It is probably due to carboxylic acid groups and hydroxyl groups on the surface of

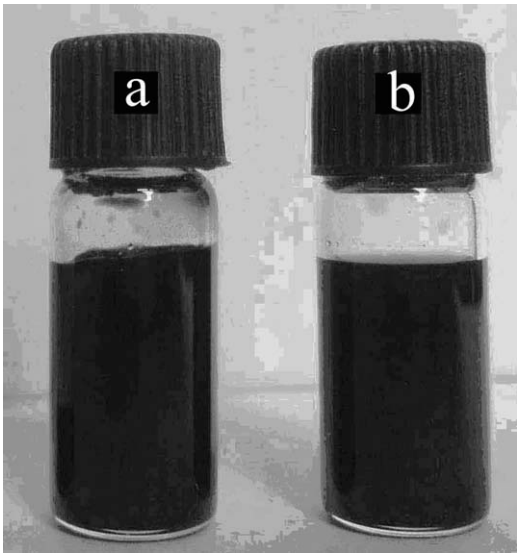

Figure 9 Photographs of purified MWNTs (a), and LC-MWNTs (b) in DMF.

MWNTs improve the compatibility of purified MWNTs and DMF. On the other hand, LC molecules on the side wall of LC-MWNTs can have good mutual solubility in DMF because of the chemical constitution (amide) similarity between LC and DMF molecules.

CONCLUSIONS

We have successfully anchored the LC molecules via their waist positions on the surface of MWNTs. The rod-like LC melts at 270°C and forms a liquid-crystalline state of smectic A phase which becomes isotropic at 284°C by POM. Both FTIR and Raman results demonstrate that the rod-like LC molecules are anchored on the surface of MWNTs via covalent linkage. HRTEM images and TGA show the surface of LC-MWNTs is covered with approximately 3–4 nm amorphous LC, and the loss-weight fraction of the LC layers is roughly estimated as 23%. The experiments of solubility demonstrate LC-MWNTs exhibits excellent suspension stability in DMF. LC-MWNTs, which could have more advantages to improve the dispersion and compatibility in LC matrix, may be introduced easily into LC cells to produce new excellent MWNTs/LC composites, which would have a great of potential applications like photoconductors, light-emitting diodes, photovoltaic solar cells, sensors, optical data storage, and thin-film transistors. Further experiments are in progress and the results will be described in detail in future publications.

References

1. Iijima, S. Nature 1991, 354, 56.
2. Ajayan, P. M.; Schadler, L. S.; Giannaris, C.; Rubio, A. Adv Mater 2000, 12, 750.
3. Dalton, A. B.; Collins, S.; Munoz, E.; Razal, J. M.; Ebron, V. H.; Ferraris, J. P.; Coleman, J. N.; Kim, B. G.; Baughman, R. H. Nature 2003, 423, 703.
4. Watts, P. C. P.; Hsu, W. K.; Kroto, H. W.; Walton, D. R. M. Nano Lett 2003, 3, 549.
5. Barrau, S.; Demont, P.; Peigney, A.; Laurent, C.; Lacabanne, C. Macromolecules 2003, 36, 5187.
6. Lynch, M. D.; Patrick, D. L. Nano Lett 2002, 2, 1197.
7. Weiss, V.; Thiruvengadathan, R.; Regev, O. Langmui 2006, 22, 854.
8. Dierking, I.; Scalia, G.; Morales, P.; LeClere, D. Adv Mater 2004, 16, 865.
9. Dierking, I.; Scalia, G.; Morales, P. J Appl Phys 2005, 97, 044309.
10. Lee, W.; Chen, H. Y.; Yeh, S. L. Opt Express 2002, 10, 482.
11. Chan, R.; King, Y.; Roussel, F. Appl Phys A Mater 2007, 86, 159.
12. Koysal, O.; Okutan, M.; San, S. E.; Dabrowski, R.; Ecevit, F. N. Mater Chem Phys 2008, 109, 253.
13. Jou, W. S.; Cheng, H. Z.; Hsu, C. F. J. Alloy Compd 2007, 434–435, 641.
14. Dierking, I.; San, S. E. Appl Phys Lett 2005, 87, 233507.
15. Badaire, S.; Zakri, C.; Maugey, M.; Derre, A.; Barisci, J. N.; Wallace, G.; Poulin, P. Adv Mater 2005, 17, 1673.
16. Jiang, W.; Yu, B.; Liu, W.; Hao, J. Langmuir 2007, 23, 8549.
17. Kwon, Y. S.; Jung, B. M.; Lee, H.; Chang, J. Y. Macromolecules 2010, 43, 5376.
18. Saito, T.; Matsushige, K.; Tanaka, K. Physica B 2002, 323, 280.
19. Mickelson, E. T.; Huffman, C. B.; Rinzler, A. G.; Smalley, R. E.; Hauge, R. H.; Margrave, J. L. Chem Phys Lett 1998, 296, 188.
20. Pantarotto, D.; Partidos, C. D.; Graff, R.; Hoebeke, J.; Briand, J. P.; Prato, M.; Bianco, A. J Am Chem Soc 2003, 125, 6160.
21. Blake, R.; Gunko, Y. K.; Coleman, J.; Cadek, M.; Fonseca, A.; Nagy, J. B.; Blau, W. J. J Am Chem Soc 2004, 126, 10226.
22. Holzinger, M.; Vostrowsky, O.; Hirsch, A.; Hennrich, F.; Kappes, M.; Weiss, R.; Jellen, F. Angew Chem Int Ed 2001, 40, 4002.
23. Hu, H.; Zhao, B.; Hamon, M. A.; Kamaras, K.; Itkis, M. E.; Haddon, R. C. J Am Chem Soc 2003, 125, 14893.
24. Peng, H. Q.; Alemany, L. B.; Margrave, J. L.; Khabashesku, V. N. J Am Chem Soc 2003, 125, 15174.
25. Chen, X. H.; Wang, J. F.; Zhong, W. B.; Feng, T.; Yang, X. G.; Chen, J. H. Macromol Chem Phys 2008, 209, 846.
26. Stephenson, J. J.; Sadana, A. K.; Higginbotham, A. L.; Tour, J. M. Chem Mater 2006, 18, 4658.
27. Borondics, F.; Bokor, M.; Matus, P.; Tompa, K.; Pekker, S.; Jakab, E. Fuller Nanotub Car N 2005, 13, 375.
28. Pe'nicaud, A.; Poulin, P.; Derre, A.; Anglaret, E.; Petit, P. J Am Chem Soc 2005, 127, 8.
29. Saito, K.; Ohtani, M.; Fukuzumi, S. J Am Chem Soc 2006, 128, 14216.
30. Chen, X. H.; Chen, C. S.; Chen, Q.; Cheng, F. Q.; Zhang, G.; Chen, Z. Z. Mater Lett 2002, 57, 734.
31. Dierking, I. In Textures of Liquid Crystals; Mortensen, K., Ed. WILEY-VCH: Weinheim, 2003; p 164.
32. Yi, B.; Rajagopalan, R.; Foley, H. C.; Kim, U. J.; Liu, X.; Eklund, P. C. J Am Chem Soc 2006, 128, 11307.
33. Corrias, M.; Serp, P.; Kalck, P.; Dechambre, G.; Lacout, J. L.; Castiglioni, C.; Kihn, Y. Carbon 2003, 41, 2361.
34. Dresselhaus, M. S.; Dresselhaus, G.; Jorio, A.; Souza Filho, A. G.; Saito, R. Carbon 2002, 40, 2043.
35. Majumder, M.; Chopra, N.; Hinds, B. J. J Am Chem Soc 2005, 127, 9062.
36. Qin, Y.; Shi, J.; Wu, W.; Li, X.; Guo, Z. X.; Zhu, D. J Phys Chem B 2003, 107, 12899.